



**Fluorination and Hydrolytic Stability of Water-Soluble
Platinum Complexes with a Borane-Bridged
Diphosphoramidite Ligand**

Journal:	<i>Dalton Transactions</i>
Manuscript ID	DT-ART-05-2022-001482.R1
Article Type:	Paper
Date Submitted by the Author:	01-Aug-2022
Complete List of Authors:	Culpepper, Johnathan; The University of Iowa, Chemistry Lee, Kyoungsoon; Gyeongsang National University, Department of Chemical Education Portis, William; The University of Iowa, Chemistry Swenson, Dale; The University of Iowa, Chemistry Daly, Scott; The University of Iowa, Chemistry

ARTICLE

Fluorination and Hydrolytic Stability of Water-Soluble Platinum Complexes with a Borane-Bridged Diphosphoramidite Ligand

Received 00th January 20xx,
Accepted 00th January 20xx

DOI: 10.1039/x0xx00000x

Johnathan D. Culpepper,^{ab} Kyoungsoon Lee,^{ac} William Portis,^a Dale C. Swenson,^a and Scott R. Daly^{a†}

The high fluorophilicity of borane-containing ligands offers promise for accessing new metallodrug candidates capable of bifunctional [¹⁸F]-positron emission tomography (PET) imaging, but this requires water soluble and hydrolytically stable ligands that can be fluorinated under mild conditions. Toward this goal, here we report the synthesis and characterization of water-soluble Pt(II) complexes containing a triaminoborane-bridged diphosphoramidite ligand called Me^oTBDPhos that can be fluorinated using simple fluoride salts. NMR and XRD studies show that (Me^oTBDPhos)PtCl₂ (**1**) dissolves in water with cooperative H-OH addition across the bridgehead N-B bond to form **1-H₂O**. The B-OH bond in **1-H₂O** undergoes rapid displacement with fluoride (<10 min) when treated with CsF in MeCN to form **1-HF**. **1-HF** can also be prepared in <10 min by addition of KF to **1** in the presence Kryptofix[®] 222 and (HNEt₃)Cl in MeCN. In addition to using fluoride salts, we show how mononuclear **1** can be fluorinated with HBF₄·Et₂O to form dinuclear [(Me^oTBDPhos-HF)Pt(μ-Cl)]₂(BF₄)₂ (**4-HF**). Comparative studies show that the B-F bond in **1-HF** undergoes hydrolysis as soon as it is dissolved in water or saline, but the B-F bond persists for hours when the pH of the solution is lowered to pH ≤ 2. In contrast to **1-HF**, the B-F bond in dinuclear **4-HF** persists for days when dissolved in water, which may be attributed to slow, sacrificial release of fluoride from the BF₄⁻ anion. The results show how cooperative N-B reactivity on the ligand can be leveraged to rapidly fluorinate water-soluble Me^oTBDPhos complexes under mild conditions and afford suggestions for how to enhance hydrolytic B-F stability, as required for use in biomedical applications.

Introduction

FDA-approved platinum drugs cisplatin, carboplatin, and oxaliplatin are among the most widely used and important chemotherapeutic agents available in the treatment of cancer (Chart 1).¹ However, despite their remarkable efficacy, these metallodrugs have notoriously severe side effects due to off-target accumulation in healthy cells and tissues.² Furthermore, some cancer cell lines are resistant to traditional platinum-based metallodrugs.³ These issues have continued to stimulate the hunt for new metallodrugs with attenuated side effects.⁴

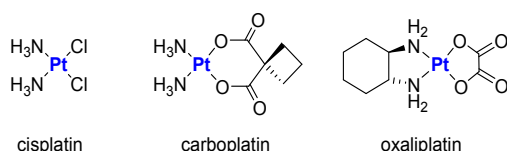


Chart 1. FDA-approved Pt metallodrugs.

^a Department of Chemistry, The University of Iowa, E331 Chemistry Building, Iowa City, Iowa 52242, United States.

^b Current address: Corning Incorporated, Corning, NY 14831, United States.

^c Current address: Department of Chemical Education and Research Institute of Natural Sciences, Gyeongsang National University, Jinju 52828, Republic of Korea.

† Corresponding Author: scott-daly@uiowa.edu.

Electronic Supplementary Information (ESI) available: CCDC 1958363, 2172270-2172271. Experimental details and tabulated crystallographic data. NMR and IR spectra. See DOI: 10.1039/x0xx00000x.

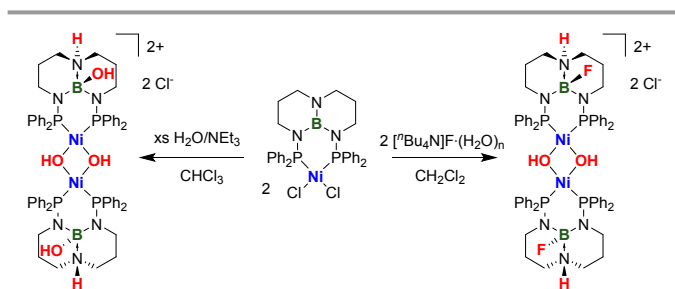
A challenge impeding the search for more effective metallodrugs is the painstaking and time-consuming approach of identifying how chemical modifications affect metallodrug biodistribution in healthy and malignant tissues. Traditional methods have relied on injecting different metallodrug candidates into animals and then harvesting tissues after euthanization.⁵ Not only does this make it impossible to compare drug distribution and longer-term treatment efficacy in the same animal, it is not feasible for clinical studies; analysis of metallodrug distribution in humans is more challenging because it requires tissue samples to be removed surgically, risking additional harm to the patient. For this reason, clinical studies have been limited primarily to single-time point analysis of drug localization in excised tumor tissues, as demonstrated with patients afflicted with non-small-cell lung and bladder cancers.⁶

A method that could provide a non-invasive, time-resolved approach to monitoring how chemical modifications to metallodrugs affect their biodistribution *in vivo* is positron emission tomography (PET) imaging.⁷ The key advantage of PET imaging over other imaging modalities is that emitted radiation can be detected outside the patient, even through dense tissues.⁸ Of the isotopes available, [¹⁸F] PET imaging is the most commonly used method for clinical cancer imaging with radiopharmacies and on-site cyclotrons providing ¹⁸F to hospitals worldwide.^{8,9} However, despite its prolific clinical use,

[^{18}F] PET imaging has rarely been used for imaging anti-cancer metallodrugs because it requires rapid fluorine labeling protocols that can accommodate the relatively short half-life of ^{18}F ($t_{1/2} = 110$ min). Moreover, this approach requires a unique ^{18}F radiolabeling protocol to be developed for each drug candidate. Despite these challenges, the high promise of this metallodrug imaging approach was demonstrated with a ^{18}F -labeled derivative of carboplatin that was prepared in a multistep synthesis.¹⁰

Rather than developing new ^{18}F labeling protocols for each metallodrug candidate, an alternative approach is to develop metallodrugs that contain highly tunable and modular ligands that 1) can be rapidly labeled with fluoride using an automatable protocol, and 2) form complexes with a wide range of transition metals of interest for metallodrug use (e.g., Ru, Ir, Au).¹¹ This would help collapse the drug discovery timeline and allow clinical imaging to take place during treatment to ensure that the drug is delivered to malignant sites.

With these ideas in mind, we have been investigating a class of diphosphorus ligands called TBDPhos that contain a triaminoborane backbone derived from 1,8,10,9-triazaboradecalin (TBD).¹² Most of our work to date has centered on TBDPhos ligands with phenyl substituents attached to phosphorus ($^{\text{Ph}}\text{TBDPhos}$). We have shown that this ligand can undergo cooperative ligand-centered reactions¹³ at the TBD backbone in the presence of Brønsted acids when bound to different transition metals. For example, addition of H_2O , or hydrated ($^n\text{Bu}_4\text{N}$)F to ($^{\text{Ph}}\text{TBDPhos}$)NiCl₂ in organic solvents resulted in net H-OR (R = H) or H-X addition (where X = F) across the bridgehead N-B bond (Scheme 1).^{13, 14} Similar ligand-centered reactivity has been observed in $^{\text{Ph}}\text{TBDPhos}$ complexes containing Pd, Pt, Cu, and Mo.^{15, 16} As we will discuss in more detail below, a key feature of this reactivity is protonation of the bridgehead nitrogen, which dramatically enhances Lewis acidity at boron via N-B cooperativity.¹⁷



Scheme 1. Ligand-centered reactions previously reported with ($^{\text{Ph}}\text{TBDPhos}$)NiCl₂ in non-aqueous solvents.¹³

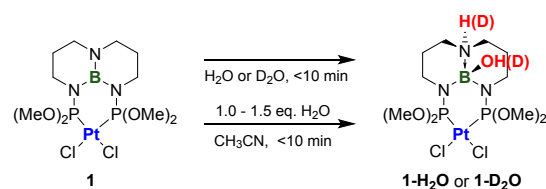
Our prior results suggested that TBDPhos complexes could potentially be used as metallodrug candidates for ^{18}F imaging studies provided that water-soluble derivatives could be prepared and rapidly fluorinated using simple fluoride salts like those obtained from ^{18}F radiopharmacies (e.g., K^{18}F).¹⁸ Water soluble complexes containing phosphorus ligands have shown as potential anticancer metallodrugs.¹⁹ We recently showed that changing the phenyl substituents in $^{\text{Ph}}\text{TBDPhos}$ to methoxy in $^{\text{MeO}}\text{TBDPhos}$ enhances ligand-centered reactivity in Pt TBDPhos complexes in side-by-side comparisons.¹⁶ This is

notable because it has been reported that adding methoxy substituents to P(III) is an effective strategy for imparting water solubility to metal complexes containing diphosphorus ligands.²⁰ Consistent with these prior results, we show here that ($^{\text{MeO}}\text{TBDPhos}$)PtCl₂ is indeed water soluble, and we demonstrate how it can be fluorinated under mild conditions using simple fluoride salts (KF and CsF). We also describe alternative fluorination methods using $\text{HBF}_4\cdot\text{Et}_2\text{O}$ and discuss how pH affects hydrolytic B-F stability in water and saline.

Results and discussion

Hydrolysis studies with ($^{\text{MeO}}\text{TBDPhos}$)PtCl₂ and [($^{\text{MeO}}\text{TBDPhosPt}$)₂($\mu\text{-Cl}$)₂](OTf)₂. We have shown previously that $^{\text{Ph}}\text{TBDPhos}$ ligands can undergo reactions in organic solvents in the presence of excess water without significant decomposition. Because of the aqueous insolubility of ($^{\text{Ph}}\text{TBDPhos}$)MCl₂ (where M = Ni or Pd), prior reactions with water were performed in biphasic $\text{CHCl}_3/\text{H}_2\text{O}$ mixtures (Scheme 1). The reactions were sluggish unless NEt_3 was added, which caused the mononuclear ($^{\text{Ph}}\text{TBDPhos}$)MCl₂ complexes to lose inner sphere chlorides and form dinuclear [($^{\text{Ph}}\text{TBDPhos-H}_2\text{O}$)M($\mu\text{-OH}$)₂Cl₂].¹³

In contrast to prior studies with $^{\text{Ph}}\text{TBDPhos}$, ($^{\text{MeO}}\text{TBDPhos}$)PtCl₂ (**1**) dissolves readily in H_2O and D_2O with rapid addition of (heavy) water to the TBD backbone (Scheme 2), as evident from NMR data collected on these solutions. The ^{11}B NMR spectrum of **1** in D_2O revealed a large shift from δ 22.7 ppm in CD_2Cl_2 to δ 0.0 ppm corresponding to the change from 3- to 4-coordinate boron and formation of ($^{\text{MeO}}\text{TBDPhos-D}_2\text{O}$)PtCl₂ (**1-D₂O**) (Table 1). The ^{31}P NMR spectrum revealed a sharp singlet at δ 65.5 ppm with the expected satellite peaks associated with $^{195}\text{Pt}\text{-}^{31}\text{P}$ coupling ($^1J_{\text{PtP}} = 4991$ Hz).



Scheme 2. Hydrolysis of ($^{\text{MeO}}\text{TBDPhos}$)PtCl₂.

^{11}B spectra collected on the water mixtures with **1-H₂O** revealed small amounts of boric acid indicating that some of the ligand is decomposed during dissolution (Figure S28; ESI). We discovered **1-H₂O** can be generated more cleanly by adding water to MeCN solutions of **1**. **1-H₂O** can be readily isolated as single-crystals from either reaction by evaporating the solvent, extracting the residue with CH_2Cl_2 , and allowing Et_2O to slowly diffuse into the filtered CH_2Cl_2 solution. XRD studies revealed that **1-H₂O** is mononuclear (Figure 1), indicating that **1** does not lose chloride and form dinuclear complexes as observed when ($^{\text{Ph}}\text{TBDPhos}$)MCl₂ complexes are dissolved in the presence of water and NEt_3 , as shown in Scheme 1. The isolated structures confirmed substantial pyramidalization of the boron atom, as observed in subporphyrins with similar (NNN)B-OH containing structures.^{21, 22} The average sum of the N-B-N angles for **1-H₂O**

(323°) are also similar to those observed in other TBDPhos complexes with four-coordinate boron.¹³ The XRD data for **1-H₂O** revealed bridgehead N-B bond distances in the range of 1.63(4) – 1.66(3) Å consistent with a dative N→B bond. For comparison, the N(P)-B bond distances are shorter at 1.53(2) – 1.55(3) Å, consistent with distances expected for covalent N-B σ bonds.

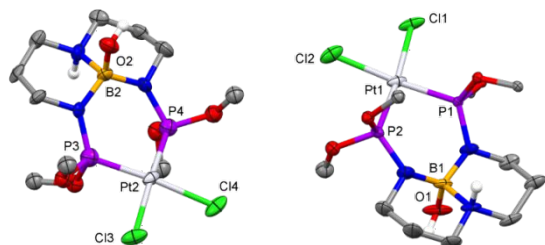


Figure 1. Molecular structure of (MeOTBDPhos-H₂O)PtCl₂ (**1-H₂O**) with thermal ellipsoids at the 50% probability level. Hydrogen atoms attached to carbon and disordered components were omitted from the figure.

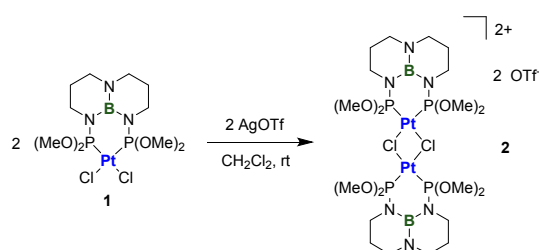
Table 1. ¹¹B, ¹⁹F and ³¹P NMR resonances and Pt-P coupling constants in CDCl₃. Chemical shifts are reported in δ units relative to BF₃·Et₂O (¹¹B; δ 0.0 ppm), 0.05% C₆H₅CF₃ in C₆D₆ (¹⁹F; δ -62.9 ppm), and 85% H₃PO₄ (³¹P; δ 0.0 ppm).

Compound	¹¹ B	¹⁹ F	³¹ P	¹ J _{PtP} (Hz)
MeOTBDPhos ^a	24.7	-	145.6	-
1 ^a	22.7	-	69.9	4895
2	22.4	-78.7 (OTf)	54.4	5253
1-D₂O ^b	0.0	-	65.5	4991
1-H₂O ^c	1.2	-	69.4	4938
2-H₂O	-0.3	-78.8 (OTf)	50.5	5246
1-HF (Method 1) ^c	1.2	-166.7	69.2	4935
1-HF (Method 2)	0.8	-167.3	69.2	4918
3 ^d	22.3	-	60.7	4882
3-HF (Method 2)	1.1	-167.0	59.5	4903
4-HF	0.3	-167.7	51.8	5250
	-1.3 (BF ₄)	-151.8 (BF ₄)	-	-

^aRef. ¹⁶. ^bData collected in D₂O. ^cData collected in CD₃CN. ^dRef. ²³.

Given that TBDPhos complexes are known to sometimes form dinuclear species in the presence of water, we sought a dinuclear complex for comparative hydrolysis and fluorination testing with mononuclear **1**. Reacting **1** with AgOTf resulted in the dinuclear complex [(MeOTBDPhosPt)₂(μ-Cl)₂](OTf)₂ (**2**; Scheme 3), which was isolated in high crystalline yield (83%). The only significant difference in the NMR data for dinuclear **2** compared to mononuclear **1** was a shift in the ³¹P resonance from δ 69.9 ppm (**1**) to δ 54.4 ppm (**2**) and an increase in the ¹J_{Pt-P} coupling from 4895 to 5253 Hz, respectively (Table 1). As discussed in the hydrolysis studies below, these diagnostic ³¹P chemical shifts and Pt-P coupling constants played a pivotal role in assigning the nuclearity of the complexes in aqueous mixtures.

The dinuclear structure of **2** was confirmed by single-crystal XRD studies (Figure 2). The geometry around both metals is square planar, but the structure adopts a puckered, butterfly-shaped Pt₂Cl₂ core with an angle of 138.6° between the Pt wingtips and the bridging Cl...Cl hinge. This puckered geometry is rare for chloride-bridge Pt dimers, and only a handful of examples are known in the literature.²⁴ As described by Alemany and coworkers in more general studies of edge-sharing dinuclear d⁸ complexes,²⁵ the bent structure of **2** is likely a consequence of the strong σ-donor and π-acid properties of MeOTBDPhos with Pt and the small steric profile of the methoxy substituents (bulky phosphorus substituents attenuate formation of the puckered Pt₂Cl₂ core when there is an electronic preference). The sp² hybridized boron atoms in each complex assume the expected trigonal planar geometry with Σ(N-B-N) = 360°. The bridgehead N-B bond distances are around the expected distance of 1.40 Å, whereas the (P)N-B bond distances are 0.04 – 0.08 Å longer. The remaining bond lengths are relatively unremarkable compared to other PtCl₂ complexes with phosphoramidite ligands (Table 2).²⁶



Scheme 3. Synthesis of **2**.

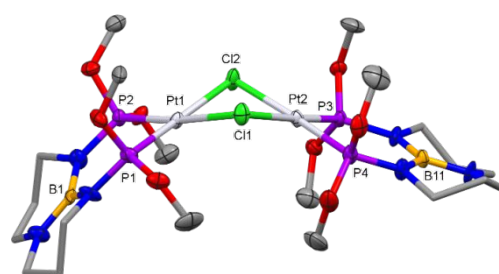


Figure 2. Molecular structure of [(MeOTBDPhos)Pt(μ-Cl)]₂(OTf)₂ (**2**). Ellipsoids are drawn at 50% probability. Hydrogen atoms attached to carbon and triflate anions were omitted from the figure.

Dissolving dinuclear **2** in water or MeCN/H₂O solutions resulted in H-OH across the TBD backbone, as observed with **1**. However, ³¹P NMR data collected on these solutions revealed a mixture of resonances including those consistent with mononuclear **1-H₂O** and dinuclear **2-H₂O** based on their chemical shifts and ¹J_{Pt-P} coupling constants. Layering CDCl₃ or CH₂Cl₂ solutions of **2** with water to form biphasic CDCl₃/H₂O or CH₂Cl₂/H₂O mixtures allowed **2-H₂O** to be formed more cleanly based on NMR data, but the product was not pure enough to give satisfactory elemental analysis. The ³¹P NMR spectrum of **2-H₂O** in CDCl₃ revealed a chemical shift of δ 50.5 ppm with ¹J_{Pt-P} = 5246 Hz indicating that it remains dinuclear in solution (Table 1).

Fluorination studies of mononuclear complexes. The ^{18}F isotope has a $t_{1/2} = 110$ min, which necessitates the need for rapid fluorination methods for complexes if they are to be used for positron emission tomography (PET) imaging. As mentioned above, ^{18}F used for PET imaging studies is typically isolated from cyclotrons as alkali metal salts, so direct fluorination using KF or CsF would be the most advantageous for potential imaging studies.

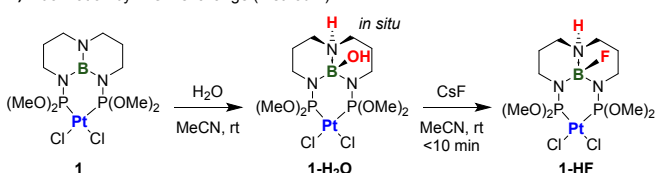
Our first boron fluorination method (Scheme 4a; Method 1) used **1-H₂O** as the starting material. These complexes are ideal because they can be handled in air because are already hydrolyzed, but it was not clear if the B-OH bond could be directly substituted with simple fluoride salts under mild conditions. Indeed, it has been shown that B-OH containing subporphyrins require harsher fluorination conditions such as addition of excess $\text{BF}_3 \cdot \text{OEt}_2$ to induce B-OH for B-F exchange.²⁷

Table 2. Selected bond distances (Å) and angles (°) from single-crystal XRD data.

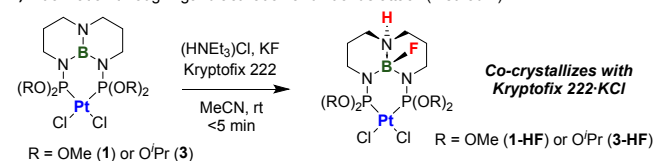
	M-P	M-Cl	N-B	(P)N-B	P-N	B-O/B-F	P-M-P	Σ NBN
1^a	2.1925(6)	2.3573(6)	1.409(5)	1.457(3)	1.649(2)		97.47(3)	360.0(2)
1-H₂O^b	2.16(1)	2.378(7)	1.66(3)	1.53(2)	1.63(2)	1.44(2)	92.1(3)	323(2)
	2.261(7)	2.373(7)		1.53(2)	1.65(2)			
	2.17(2)	2.370(9)	1.66(3)	1.53(2)	1.64(2)	1.44(2)	88.3(7)	323(2)
	2.24(1)	2.381(7)		1.53(2)	1.63(3)			
2	2.190(3)	2.399(3)	1.40(2)	1.44(2)	1.63(1)	-	91.5(1)	359(1)
	2.194(3)	2.404(3)	1.40(2)	1.46(2)	1.63(1)		96.6(1)	360(1)
	2.198(3)	2.406(3)		1.46(2)	1.63(1)			
	2.200(3)	2.410(3)		1.48(2)	1.63(1)			
3^c	2.201(1)	2.359(1)	1.400(6)	1.449(6)	1.658(4)	-	96.17(4)	360.0(7)
	2.194(1)	2.353(1)		1.460(6)	1.653(4)			
3-HF^b	2.203(2)	2.366(2)	1.635(7)	1.524(8)	1.632(4)	1.419(7)	97.10(6)	329.7(8)
	2.207(1)	2.366(2)		1.523(9)	1.630(5)			
	2.206(2)	2.366(2)	1.62(1)	1.51(1)	1.623(6)	1.423(9)	97.39(7)	332(1)
	2.199(2)	2.364(2)		1.527(9)	1.633(6)			

^aReference ¹⁶ ^bTwo molecules in the asymmetric unit. ^cReference ²³.

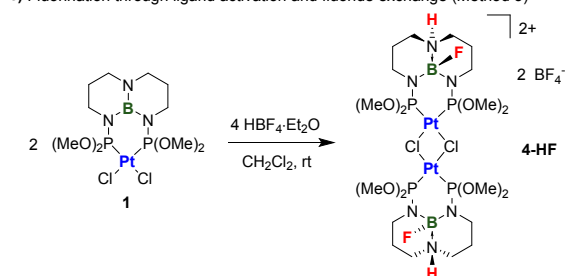
a) Fluorination by B-OH exchange (Method 1)



b) Fluorination through ligand activation and fluoride attack (Method 2)



c) Fluorination through ligand activation and fluoride exchange (Method 3)



Scheme 4. Summary of fluorination protocols.

Addition of CsF to **1-H₂O** in MeCN resulted in a rapid exchange of B-OH for B-F to form $(^{\text{MeO}}\text{TBDPhos-HF})\text{PtCl}_2$ (**1-HF**), as evident by an immediate color change from colorless to faint yellow and a diagnostic B-F resonance in the ^{19}F NMR spectrum at δ -166.7 ppm (Figure 3). For reference, the ^{19}F resonance for free fluoride appears at δ -119.0 ppm in MeCN (similar to that shown below in water).²⁸

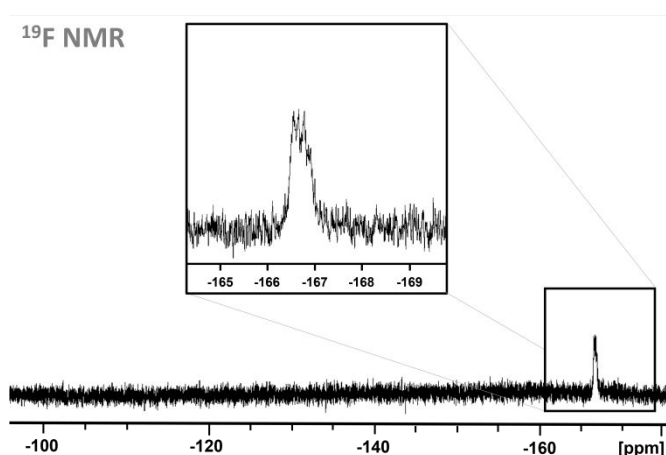


Figure 3. ^{19}F NMR spectrum collected <10 min after addition of CsF to **1-H₂O** in MeCN. ^{11}B and ^{31}P NMR spectra are shown in the ESI.

Unfortunately, attempts to cleanly isolate **1-HF** from the reaction mixtures were unsuccessful. Consistent with our hydrolysis studies described below, it appears that **1-HF** slowly reverts to **1-H₂O** upon workup due to the presence of residual water remaining in the solvent. We therefore developed a second approach to directly fluorinate the parent complex **1** under anhydrous conditions (Scheme 4b; Method 2).

Informed by previous reactivity studies, a major requirement for ligand-centered TBDPhos reactivity is protonation of the bridgehead N-B nitrogen.¹³⁻¹⁶ To address this requirement in an aprotic solvent, we used (HNEt₃)Cl as a proton source. Treating **1** with (HNEt₃)Cl in MeCN, followed by addition of KF resulted in no H-F addition to the TBD backbone over the course of 3 days. However, repeating the reaction using the cryptand Kryptofix[®] 222, which is known to abstract the potassium from KF and yield a more nucleophilic fluoride anion [F⁻], resulted in an immediate reaction to form **1-HF**. Incidentally, ¹⁸F PET imaging drugs are often prepared in MeCN using a labeling protocol that relies on K¹⁸F and Kryptofix[®] 222.²⁹

1-HF was isolated by vapor-diffusion crystallization with CH₂Cl₂ and Et₂O. ¹H and ¹³C NMR spectra and elemental analysis data collected on the crystal revealed that **1-HF** prepared this way co-crystallizes with Kryptofix 222-KCl. The ¹H and ¹³C NMR data revealed two resonances for the MeO groups due to the asymmetry caused by *trans* H-F arrangement at the TBD backbone (similar splitting of the propylene CH₂ resonances is observed in the ¹H NMR spectrum). The ¹¹B and ³¹P resonances in CDCl₃ are not remarkably different from those observed for **1-H₂O** in MeCN (Table 1), but the ¹⁹F resonance at δ -167.3 ppm confirmed the presence of the new B-F bond.

Repeated attempts to collect XRD data on crystals of **1-HF** to verify the structure were unsuccessful. However, we discovered that the same fluorination method with KF and Kryptofix 222 could be used with the closely related complex (iPr^oTBDPhos)PtCl₂ (**3**).²³ This complex is not appreciably soluble in water due to the more lipophilic isopropyl groups (i.e. not useful for aqueous applications), but it yielded X-ray quality crystals of (iPr^oTBDPhos-HF)PtCl₂ (**3-HF**) to structurally confirm successful addition of fluoride (Figure 4).

3-HF was prepared in the same way as **1-HF** using **3** and isolated as single crystals in 61% yield. As with **1-HF**, NMR and EA studies of **3-HF** revealed that it co-crystallizes with Kryptofix 222-KCl, which was confirmed by XRD studies. The structure revealed the expected *trans* H-F addition across the B-F bond with B-F distances of 1.421(7) and 1.424(9) Å. As with **1-H₂O**, the most significant change in the structures of **3-HF** compared to that reported previously for **3** was the N-B bond distances and the N-B-N angles, which show the expected lengthening and pyramidalization, respectively, due to the change from three- to four-coordinate boron. The remaining bond distances and angles for **3-HF** are similar to those reported previously for **3**.²³

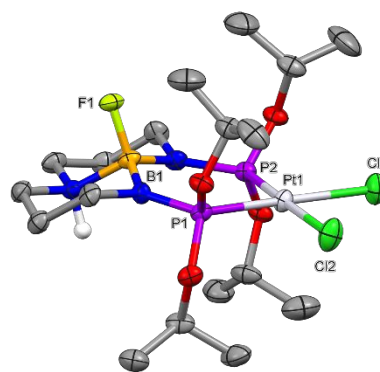


Figure 4. Molecular structure of [(iPr^oTBDPhos-HF)PtCl₂ (**3-HF**). Ellipsoids are drawn at 50% probability. Hydrogen atoms attached to carbon, co-crystallized Kryptofix 222-KCl, and a second molecule of **3-HF** in the asymmetric unit cell were omitted from the figure.

Fluorinated dinuclear complexes. Fluorination Methods 1 and 2 in Scheme 4 were unsuccessful when we attempted to prepare [(^{Me}O)TBDPhosPt(HF)(μ-Cl)]₂(OTf)₂ (**2-HF**) using **2-H₂O** or **2**, respectively. The dinuclear complexes appear to break up into a mixture of products with these methods, and we have only successfully recovered crystals of fluorinated and mononuclear **1-HF** from the reaction mixtures. As such, we began exploring other methods to prepare a fluorinated dinuclear complex for side-by-side hydrolysis comparison to **1-HF**.

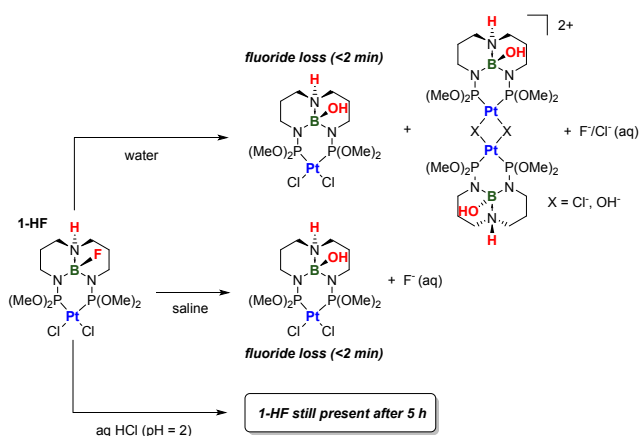
We have shown previously that treating (P^hTBDPhos)NiCl₂ with two equiv. of HBF₄·Et₂O in Et₂O results in H-F addition across the TBD backbone and formation of dinuclear [(P^hTBDPhos-HF)Ni(μ-Cl)]₂(BF₄)₂.¹⁴ Here we report that performing this same reaction with **2** affords [(^{Me}O)TBDPhos-HF)Pt(μ-Cl)]₂(BF₄)₂ (**4-HF**) (Scheme 4c; Method 3). The isolated crystals of **4-HF** were highly deliquescent and not suitable for XRD studies. However, the ³¹P NMR data revealed a resonance at δ 51.8 ppm (¹J_{PtP} = 5250 Hz) similar to dinuclear complexes **2** and **2-H₂O**. Two resonances were observed in the ¹¹B NMR spectrum at δ 0.3 and -1.3 ppm, as well as two in the ¹⁹F NMR spectrum at δ -167.7 and -151.8 corresponding to the F-bound TBDPhos complex and [BF₄⁻] counter anions, respectively.¹⁴ These chemical shifts are similar to those observed for [(P^hTBDPhos-HF)Ni(μ-Cl)]₂(BF₄)₂.¹⁴

B-F hydrolytic stability studies. In addition to common challenges like low aqueous solubility, there are few boron-containing complexes that maintain B-F bonds when dissolved in aqueous environments.^{30,31} Most that tend to be stable in the presence of water are those containing B-aryl substituents or bodipy-like structures, and some of these have been used successfully in ¹⁸F PET imaging studies in mice.^{31,32}

To evaluate the hydrolytic stability of the B-F bond in **1-HF**, we dissolved this Pt complex in water and saline and monitored the solutions by ¹⁹F, ³¹P and ¹¹B NMR spectroscopy (Figure S30; ESI). Unfortunately, the B-F bond hydrolyzed in less than a minute to form B-OH in both water and saline. This was confirmed by loss of the ¹⁹F resonance associated with the B-F bond and a new resonance at δ -119.0 ppm for free fluoride.²⁸

The ^{11}B NMR spectra showed a subtle, but diagnostic shift associated with exchange from B-F to B-OH. Unlike the experiments dissolving **1** in water, no boric acid associated with ligand decomposition was observed within the first 30 min.

One distinction that is observed when dissolving **1-HF** in water vs. saline is differing amounts of mononuclear and dinuclear species present in solution (Scheme 5). The ^{31}P NMR spectra of the water solutions revealed mixtures of mononuclear and dinuclear products, as indicated by the chemical shifts at δ 64.9 and 58.5 ppm. In contrast, only mononuclear **1-H₂O** was observed in saline. Not surprisingly, this indicates that the presence of additional chloride from NaCl attenuates Pt-Cl chloride loss and formation of dinuclear complexes.



Scheme 5. Summary of hydrolysis experiments with **1-HF**.

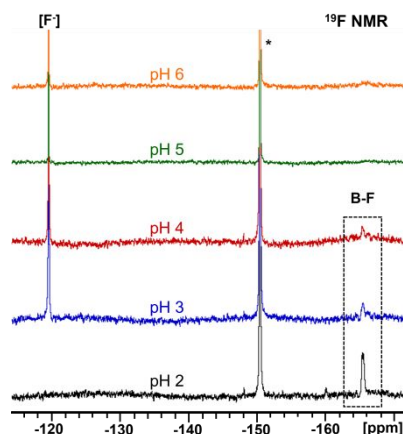


Figure 5. ^{19}F NMR spectra collected immediately after dissolving **1-HF** in water at different pH, as adjusted with HCl and NaOH. The asterisk indicates the resonance associated with the $(^t\text{Bu}_3\text{PH})\text{BF}_4$ reference (sealed capillary).

We next evaluated the influence of solution pH on B-F bond stability. Dissolving **1-HF** in water and saline solutions with pH lowered in stepwise increments from 6.0 to 2.0 using HCl revealed that the B-F bond is stabilized as the concentration of acid is increased (Figure 5). At pH = 2.0, free fluoride was no longer observed by ^{19}F NMR spectroscopy, and time-resolved studies revealed that the B-F resonance at δ -165.4 ppm was still present after 5 h (Figure 6). The ^{11}B and ^{31}P NMR spectra also

showed the expected resonances for mononuclear **1-HF** over this time interval, and only a small amount of boric acid was observed in the ^{11}B NMR spectra. Moreover, the ^{31}P NMR spectrum showed no presence of a dinuclear complex present once the pH was lowered to 2.0. As when **1-HF** is dissolved in saline, we attribute the lack of dinuclear complexes to the presence of additional chloride from HCl. Consistently, the results obtained in water were effectively the same with saline adjusted to $\text{pH} \leq 2$ (Figure 4).

We next investigated if fluoride displaced upon dissolving **1-HF** in water or saline could be added back to the TBD backbone by simply lowering the pH of the solution. Dissolving **1-HF** in saline at pH = 5 (adjusted with HCl) resulted in rapid hydrolysis to form **1-H₂O**, as described above. Adding several drops of aqueous HCl to lower the pH (< 2) and subsequent monitoring by ^{11}B and ^{19}F NMR spectroscopy revealed significant formation of boric acid indicative of decomposition (Figure S35; ESI). Only negligible amounts of **1-HF** were observed. Collectively, these results suggest that the B-F is unlikely to reform to an appreciable extent in aqueous environments at low pH once fluoride is lost.

The B-F hydrolysis studies with mononuclear **1-HF** revealed that the complex loses chloride to form dinuclear species when no additional source of chloride is present (*i.e.* NaCl or HCl). With this observation in mind, we investigated B-F hydrolysis starting with dinuclear **4-HF** to determine if it was less susceptible to B-F hydrolysis when dissolved in water or D_2O . Unlike studies with **1-HF**, NMR data collected after dissolving **4-HF** revealed that the B-F bond on the TBD backbone persists for up to 48 h (Figure 7). Some decomposition does occur, as indicated by the presence of boric acid, and several new features are observed in the ^{19}F and ^{11}B NMR spectra consistent with B-F hydrolysis products of the formula $[\text{BF}_n(\text{OH})_{n-1}]^{1-}$.³³

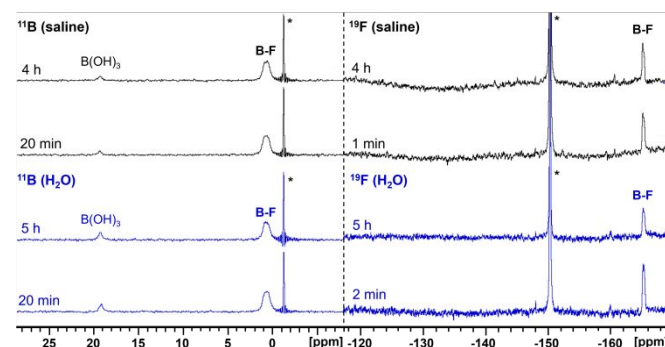


Figure 6. Time-resolved ^{11}B and ^{19}F NMR spectra of **1-HF** in water adjusted to pH 2.0 (bottom traces in blue) and in 0.9% saline solution at pH 1.5 (top traces in black). The asterisks indicate peaks associated with the $(^t\text{Bu}_3\text{PH})\text{BF}_4$ reference (sealed capillary).

The ^{31}P NMR spectra revealed that most of the dinuclear complex converts into a mononuclear complex, which likely occurs through ligand disproportionation involving water and/or hydroxide ligands. The $^1\text{J}_{\text{Pt-P}}$ coupling constant of 4908 Hz associated with the mononuclear complex resonance at δ 66.5 ppm is ~ 80 Hz smaller than that observed for **1-D₂O** in D_2O (Table 1), which may suggest that the ancillary ligands are no

longer chloride. Even more significant, the $^1J_{\text{Pt-P}}$ coupling constant of 5424 Hz for the dinuclear resonance at δ 52.0 ppm is ca. 180 Hz larger than that observed for either **3-H₂O** or **4-HF** in CDCl₃. This larger change in coupling constant suggests that the chloride ligands have been exchanged for hydroxide to form $[(^{\text{MeO}}\text{TBDPhos-HF})\text{Pt}(\mu\text{-OH})]_2^{2+}$, as observed in previous studies with Ni and Pd.¹³ Another possibility is that the chloride ligands exchanged for fluoride instead of hydroxide, but we did not observe any ^{19}F resonances consistent with those expected for Pt-F bonds.

The attenuation of hydrolysis when **4-HF** is dissolved in water is unusual given that a mononuclear species similar to **1-HF** is formed, and because **1-HF** immediately loses fluoride

when dissolved in water close to neutral pH to form **1-H₂O**. This suggests that the B-F containing side products formed upon dissolving **4-HF** in water (which were not observed in hydrolysis studies with **1-HF**) may assist in attenuating hydrolysis. Moreover, the presence of these species may be mediated by the hydrolysis of the BF₄⁻ counter anion, which is known to occur slowly in aqueous solution.³³ We have so far been able to obtain a fluorinated and water-soluble dinuclear complex like **4-HF** with a counter anion other than BF₄⁻ to test this hypothesis. As mentioned above, attempts to fluorinate dinuclear **3** with triflate counter ions only yielded mixtures from which mononuclear **1-HF** was isolated.

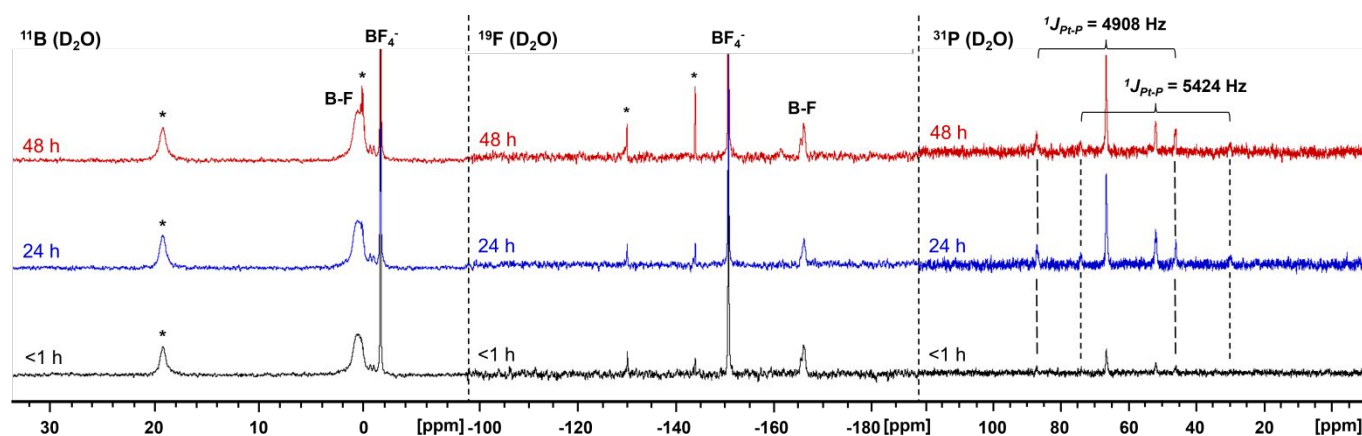


Figure 7. ^{11}B , ^{19}F , and ^{31}P NMR spectra collected over 48 h for a solution of **4-HF** in D₂O. The asterisk symbols indicate resonances assigned to boric acid and B-F containing decomposition products.

Conclusions

In summary, we have described the hydrolysis reactivity of water-soluble $(^{\text{MeO}}\text{TBDPhos})\text{PtCl}_2$ (**1**) and $[(^{\text{MeO}}\text{TBDPhos})\text{Pt}(\mu\text{-Cl})]_2(\text{OTf})_2$ (**2**). These complexes rapidly react with water upon dissolving to form $(^{\text{MeO}}\text{TBDPhos-H}_2\text{O})\text{PtCl}_2$ (**1-H₂O**) and $[(^{\text{MeO}}\text{TBDPhos-H}_2\text{O})\text{Pt}(\mu\text{-Cl})]_2(\text{OTf})_2$ (**2-H₂O**). These complexes exhibit small amounts of boric acid indicative of decomposition when dissolved, but hydrolysis reactions performed in MeCN generated **1-H₂O** and **2-H₂O** without significant decomposition.

We successfully developed two rapid fluorination protocols to add fluoride to the TBD backbone using simple salts like those obtained for ^{18}F from cyclotrons. The first protocol involved B-OH for B-F exchange using **1-H₂O** and CsF in MeCN to form **1-HF**. The mild conditions are especially notable given that exchanging B-OH bonds for B-F in subporphyrins (which have a BN₃ core similar to TBDPhos, but cannot undergo cooperative N-B reactions)²² requires harsher fluorination reagents such as BF₃·Et₂O.²⁷ However, the B-F bond in **1-HF** hydrolyzes to reform **1-H₂O** in the presence of any residual water. To circumvent this issue, we showed how **1-HF** could be prepared under anhydrous conditions by treating **1** with KF, Kryptofix 222, and (HNEt₃)Cl. A third fluorination protocol using HBF₄·Et₂O was also used to prepare the dinuclear Pt complex **4-HF**.

The results show how cooperative ligand-centered reactivity¹³ can be used to rapidly label metalated boron ligands like TBDPhos with simple fluoride salts under mild conditions – an important requirement for use with ^{18}F because of its short half-life. Unfortunately, the advantages that cooperative ligand-centered reactivity offer in terms of rapid fluoride labeling also appear to account for the rapid B-F hydrolysis observed when **1-HF** is dissolved in water or saline. However, we showed how reducing the pH of the aqueous solutions to ≤ 2 using HCl stabilization of the B-F bond at low pH suggests that maintaining protonation of bridgehead N on the TBD backbone (or subsequent replacement with a less labile substituent post fluorination) is key to maintaining the B-F bond once fluoride is added. This hypothesis offers a potential path forward for enhancing B-F bond stability under aqueous conditions, as required for use in ^{18}F imaging studies. We are currently investigating ligand modifications and related chemistries that leverage this insight to stabilize the B-F bond in TBDPhos complexes under physiologically relevant conditions and extend this chemistry to other metals being investigated for metallodrug applications.

Author Contributions

JDC, KL, and WP contributed to the investigation, conceptualization, and formal analysis, and JDC provided the

original draft of the manuscript. DCS collected the XRD data and modeled disorder in the crystal structures. SRD administered and supervised the project, acquired funding, and edited manuscript drafts. All authors have reviewed and given approval to the final version of the manuscript.

Conflicts of interest

There are no conflicts to declare.

Acknowledgements

This work was generously supported by the University of Iowa Center for Health Effects of Environmental Contamination (CHEEC), the American Chemical Society's Petroleum Research Fund (55989-DNI3), and National Science Foundation Graduate Research Fellowship Program NSF-GRFP under Grant No. (000390183) to JDC. Some of the crystallographic data within this study was collected using the instrument supported by NSF CHE-1828117. Any opinions, findings, and conclusions or recommendations expressed in this material are those of the authors and do not necessarily reflect views of the National Science Foundation.

Notes and references

1. T. W. Hambley, *Coord. Chem. Rev.*, 1997, **166**, 181-223; R. S. Go and A. A. Adjei, *J. Clin. Oncol.*, 1999, **17**, 409-422; J. L. Misset, H. Bleiberg, W. Sutherland, M. Bekradda and E. Cvitkovic, *Crit. Rev. Oncol. Hematol.*, 2000, **35**, 75-93.
2. D. M. Cheff and M. D. Hall, *J. Med. Chem.*, 2017, **60**, 4517-4532; R. Oun, Y. E. Moussa and N. J. Wheate, *Dalton Trans.*, 2018, **47**, 6645-6653.
3. D.-W. Shen, L. M. Pouliot, M. D. Hall and M. M. Gottesman, *Pharmacol. Rev.*, 2012, **64**, 706-721; A.-M. Florea and D. Büsselberg, *Cancers*, 2011, **3**, 1351-1371; M. D. Hall, M. Okabe, D.-W. Shen, X.-J. Liang and M. M. Gottesman, *Annu. Rev. Pharmacol. Toxicol.*, 2008, **48**, 495-535.
4. L. R. Kelland, S. Y. Sharp, C. F. O'Neill, F. I. Raynaud, P. J. Beale and I. R. Judson, *J. Inorg. Biochem.*, 1999, **77**, 111-115; N. J. Wheate, S. Walker, G. E. Craig and R. Oun, *Dalton Trans.*, 2010, **39**, 8113-8127; R. G. Kenny and C. J. Marmion, *Chem. Rev.*, 2019, **119**, 1058-1137; K. D. Mjos and C. Orvig, *Chem. Rev.*, 2014, **114**, 4540-4563; I. Yousuf, M. Bashir, F. Arjmand and S. Tabassum, *Coord. Chem. Rev.*, 2021, **445**, 214104.
5. A. V. Klein and T. W. Hambley, *Chem. Rev.*, 2009, **109**, 4911-4920; I. Ott, *Compr. Inorg. Chem. II*, 2013, **3**, 933-949.
6. E. S. Kim, J. J. Lee, G. He, C.-W. Chow, J. Fujimoto, N. Kalhor, S. G. Swisher, I. I. Wistuba, D. J. Stewart and Z. H. Siddik, *J. Clin. Oncol.*, 2012, **30**, 3345-3352; E. A. Guancial, D. Kilari, G.-Q. Xiao, S. H. Abu-Farsakh, A. Baran, E. M. Messing and E. S. Kim, *PLoS One*, 2016, **11**, e0155503/0155501-e0155503/0155510.
7. G. Muehlehner and J. S. Karp, *Phys. Med. Biol.*, 2006, **51**, R117; D. L. Bailey, M. N. Maisey, D. W. Townsend and P. E. Valk, *Positron emission tomography*, Springer, 2005.
8. L. K. Shankar, J. M. Hoffman, S. Bacharach, M. M. Graham, J. Karp, A. A. Lammertsma, S. Larson, D. A. Mankoff, B. A. Siegel and A. Van den Abbeele, *J. Nucl. Med.*, 2006, **47**, 1059-1066.
9. D. Le Bars, *J. Fluorine Chem.*, 2006, **127**, 1488-1493.
10. N. Lamichhane, G. K. Dewkar, G. Sundaresan, L. Wang, P. Jose, M. Otabashi, J.-L. Morelle, N. Farrell and J. Zweit, *J. Nucl. Med.*, 2017, **58**, 1997-2003.
11. W. Liu and R. Gust, *Coord. Chem. Rev.*, 2016, **329**, 191-213; E. Alessio, *Eur. J. Inorg. Chem.*, 2017, **2017**, 1549-1560; P. Sudhindra, S. Ajay Sharma, N. Roy, P. Moharana and P. Paira, *Polyhedron*, 2020, **192**, 114827; E. J. Anthony, E. M. Bolitho, H. E. Bridgewater, O. W. L. Carter, J. M. Donnelly, C. Imberti, E. C. Lant, F. Lermyte, R. J. Needham, M. Palau, P. J. Sadler, H. Shi, F.-X. Wang, W.-Y. Zhang and Z. Zhang, *Chem. Sci.*, 2020, **11**, 12888-12917; C. C. Konkankit, S. C. Marker, K. M. Knopf and J. J. Wilson, *Dalton Trans.*, 2018, **47**, 9934-9974; D. van der Westhuizen, D. I. Bezuidenhout and O. Q. Munro, *Dalton Trans.*, 2021, **50**, 17413-17437; N. P. E. Barry and P. J. Sadler, *Pure Appl. Chem.*, 2014, **86**, 1897-1910.
12. E. F. Rothger and K. Niedenzu, *Syn. Inorg. Metal-Org. Chem.*, 1971, **1**, 117-121; P. Fritz, K. Niedenzu and J. W. Dawson, *Inorg. Chem.*, 1965, **4**, 886-889.
13. K. Lee, C. M. Donahue and S. R. Daly, *Dalton Trans.*, 2017, **46**, 9394-9406.
14. K. Lee, C. Kirkvold, B. Vlaisavljevich and S. R. Daly, *Inorg. Chem.*, 2018, **57**, 13188-13200.
15. K. Lee, C. W. Kim, J. L. Buckley, B. Vlaisavljevich and S. R. Daly, *Dalton Trans.*, 2019, **48**, 3777-3785.
16. K. Lee, J. D. Culpepper, R. Parveen, D. C. Swenson, B. Vlaisavljevich and S. R. Daly, *Organometallics*, 2020, **39**, 2526-2533.
17. L. Greb, F. Ebner, Y. Ginzburg and L. M. Sigmund, *Eur. J. Inorg. Chem.*, 2020, **2020**, 3030-3047.
18. B. Shen, J. H. Park, T. Hjørnevik, P. W. Cipriano, D. Yoon, P. K. Gulaka, D. Holly, D. Behera, B. A. Avery and S. S. Gambhir, *Mol. Imaging Biol.*, 2017, **19**, 779-786; M. Richard, C. Truillet, V. L. Tran, H. Liu, K. Porte, D. Audisio, M. Roche, B. Jogo, S. Cholet and F. Fenaille, *Chem. Commun.*, 2019, **55**, 10400-10403; C. Y. Shiu, L. Q. Bai, R. R. Teng and A. Wolf, *J. Labelled. Compd. Rad.*, 1987, **24**, 55-64.
19. F. J. Ramos-Lima, A. G. Quiroga, B. Garcia-Serrelede, F. Blanco, A. Carnero and C. Navarro-Ranninger, *J. Med. Chem.*, 2007, **50**, 2194-2199; A. A. Nazarov and P. J. Dyson, *Catal. Met. Complexes*, 2011, **37**, 445-461; C. Mugge, C. Rothenburger, A. Beyer, H. Gorls, C. Gabbiani, A. Casini, E. Michelucci, I. Landini, S. Nobili, E. Mini, L. Messori and W. Weigand, *Dalton Trans.*, 2011, **40**, 2006-2016; M. D. Zivkovic, J. Kljun, T. Ilic-Tomic, A. Pavic, A. Veselinovic, D. D. Manojlovic, J. Nikodinovic-Runic and I. Turel, *Inorg. Chem. Front.*, 2018, **5**, 39-53; A. F. Alshamrani, T. J. Prior, B. P. Burke, D. P. Roberts, S. J. Archibald, L. J. Higham, G. Stasiuk and C. Redshaw, *Inorg. Chem.*, 2020, **59**, 2367-2378.
20. D. R. Tyler, *Inorg. Chim. Acta*, 2019, **485**, 33-41.
21. E. Tsurumaki, J. Sung, D. Kim and A. Osuka, *Angew. Chem., Int. Ed.*, 2016, **128**, 2596-2599; E. Tsurumaki, J. Sung, D. Kim and A. Osuka, *J. Am. Chem. Soc.*, 2015, **137**, 1056-1059; J. D. Virdo, L. Crandall, J. D. Dang, M. V. Fulford, A. J. Lough, W. S. Durfee and T. P. Bender, *CrystEngComm*, 2013, **15**, 8578-8586; S. y. Hayashi, J. Sung, Y. M. Sung, Y. Inokuma, D. Kim and A. Osuka, *Angew. Chem., Int. Ed.*, 2011, **50**, 3253-3256; K. Moriya, S. Saito and A. Osuka, *Angew.*

- Chem., Int. Ed.*, 2010, **49**, 4297-4300; J. R. Stork, J. J. Brewer, T. Fukuda, J. P. Fitzgerald, G. T. Yee, A. Y. Nazarenko, N. Kobayashi and W. S. Durfee, *Inorg. Chem.*, 2006, **45**, 6148-6151; Y. Inokuma, J. H. Kwon, T. K. Ahn, M. C. Yoo, D. Kim and A. Osuka, *Angew. Chem., Int. Ed.*, 2006, **45**, 961-964.
22. S. Shimizu, *Chem. Rev.*, 2017, **117**, 2730-2784.
23. J. D. Culpepper, K. Lee and S. R. Daly, *Polyhedron*, 2022, **221**, 115877.
24. S. M. M. Knapp, T. J. Sherbow, T. J. Ahmed, I. Thiel, L. N. Zakharov, J. J. Juliette and D. R. Tyler, *J. Inorg. Organomet. Polym. Mater.*, 2014, **24**, 145-156.
25. G. Aullon, G. Ujaque, A. Lledos, S. Alvarez and P. Alemany, *Inorg. Chem.*, 1998, **37**, 804-813.
26. A. M. Z. Slawin, M. Wainwright and J. D. Woollins, *J. Chem. Soc., Dalton Trans.*, 2002, 513-519; A. Bayer, P. Murszat, U. Thewalt and B. Rieger, *Eur. J. Inorg. Chem.*, 2002, 2614-2624; I. S. Mikhel, G. Bernardinelli and A. Alexakis, *Inorg. Chim. Acta*, 2006, **359**, 1826-1836; M. Guo and Q. Zhang, *Tetrahedron Lett.*, 2009, **50**, 1965-1968.
27. S. Shimizu, A. Matsuda and N. Kobayashi, *Inorg. Chem.*, 2009, **48**, 7885-7890.
28. M. Gerken, J. Boatz, A. Kornath, R. Haiges, S. Schneider, T. Schroer and K. Christe, *J. Fluorine Chem.*, 2002, **116**, 49-58.
29. G. E. Smith, H. L. Sladen, S. C. Biagini and P. J. Blower, *Dalton Trans.*, 2011, **40**, 6196-6205.
30. T. W. Hudnall, M. Melaiimi and F. P. Gabbai, *Org. Lett.*, 2006, **8**, 2747-2749; C.-W. Chiu and F. P. Gabbai, *J. Am. Chem. Soc.*, 2006, **128**, 14248-14249; T. W. Hudnall and F. P. Gabbai, *J. Am. Chem. Soc.*, 2007, **129**, 11978-11986; Y. Kim and F. P. Gabbai, *J. Am. Chem. Soc.*, 2009, **131**, 3363-3369; C. R. Wade and F. P. Gabbai, *Dalton Trans.*, 2009, 9169-9175; C. R. Wade and F. P. Gabbai, *Organometallics*, 2011, **30**, 4479-4481; M. S. Yuan, X. Du, Z. Liu, T. Li, W. Wang, E. V. Anslyn and J. Wang, *Chem. Eur. J.*, 2018, **24**, 9211-9216; Y. Zhang, X. Du, L. Chen, Z. Li, W. Wang, T. Li and M.-S. Yuan, *Spectrochim. Acta A*, 2019, **218**, 119-126.
31. Z. Li, T.-P. Lin, S. Liu, C.-W. Huang, T. W. Hudnall, F. P. Gabbai and P. S. Conti, *Chem. Commun.*, 2011, **47**, 9324-9326; Z. Li, K. Chansaenpak, S. Liu, C. R. Wade, P. S. Conti and F. P. Gabbai, *MedChemComm*, 2012, **3**, 1305-1308; D. M. Perrin, *Acc. Chem. Res.*, 2016, **49**, 1333-1343.
32. A. Paulus, P. Desai, B. Carney, G. Carlucci, T. Reiner, C. Brand and W. A. Weber, *EJNMMI Res.*, 2015, **5**, 1-9.
33. K. Kuhlmann and D. M. Grant, *J. Phys. Chem.*, 1964, **68**, 3208-3213; R. E. Mesmer and A. C. Rutenberg, *Inorg. Chem.*, 1973, **12**, 699-702; R. E. Mesmer, K. M. Palen and C. F. Baes, Jr., *Inorg. Chem.*, 1973, **12**, 89-95.

1